REFERENCES

[1] M. Dentan and B. de Cremoux, "Numerical simulation of the nonlinear response of a PIN photodiode under high illumination," *J. Lightwave Technol.*, vol. 8, pp 1137–1144, 1990.

[2] R. D. Esman and K. J. Williams, "Measurement of harmonic distortion in microwave photodetectors," *IEEE Photon. Technol. Lett.*, vol. 2, no. 7, pp. 502–504, 1990.

[3] K. J. Williams and R. D. Esman, "Observation of photodetector nonlinearities," *Electron. Lett.*, vol. 28, no. 8, pp. 731–733, 1992.

[4] R. R. Hayes and D. L. Persechini, "Nonlinearity of PIN photodetectors," *IEEE Photon. Technol. Lett.*, vol. 5, no. 1, pp. 70–72, 1993.

[5] K. J. Williams, R. D. Esman, and M. Dagenais, "Effect of high space-charge fields on the response of microwwave photodetectors," *IEEE Photon. Technol. Lett.*, vol. 6, no. 5, pp. 639–641, 1994.

[6] K. J. Williams, "Nonlinear mechanisms in microwave photodetectors operated with high intrinsic region electric fields," *Appl. Phys. Lett.* vol. 65, no. 10, pp. 1219–1221, 1992.

[7] I. S. Ashour, J. Harari, J. P. Vilcot, and D. Decoster, "High optical power nonlinear dynamic response of AlInAs/GaInAs MSM photodiode," *IEEE Trans. Electron Devices*, vol. 42, no. 5, pp. 828–834, 1995.

[8] A. R. Williams, A. L. Kellner, A. L. Jiang, and P. K. L. Yu, "InGaAs/InP waveguide photodetector with high saturation intensity," *Electron. Lett.*, vol. 28, no. 24, pp. 2258–2259, 1992.

[9] A. R. Williams, A. L. Kellner, and P. K. L. Yu, "High frequency saturation measurements of an InGaAs/InP waveguide photodetector," *Electron. Lett.*, vol. 29, no. 14, pp. 1298–1299, 1993.

[10] D. Wake, N. G. Walker, and I. C. Smith, "Zero-bias edge coupled InGaAs photodiodes in millimeter wave radio fiber systems," *Electron. Lett.*, vol. 29, no. 21. pp. 1879–1881, 1993.

[11] C. Dalle and P. A. Rolland, "Drift-diffusion versus energy model for millimeter wave IMPATT diodes modeling," *Int. J. Numerical Modeling: Electronic Networks, Devices and Fields*, vol. 2, no. 1, pp. 61–73, 1989.

[12] T. P. Pearsall, *GaInAsP alloy semiconductors.* New York: Wiley, 1982.

[13] S. R. Forrest, P. H. Schmidt, R. B. Wilson, and L. Kaplan, "Relationship between the conduction band discontinuities and bandgap differences in InGaAsP/InP heterojunctions," *Appl. Phys. Lett.*, vol. 45, no. 8, pp. 1199–1202, 1984.

[14] J. Schlafer, C. B. Su, W. Powazinik, and R. B. Lauer, "20 GHz bandwidth InGaAs photodetector for long wavelength microwave optical links," *Electron. Lett.*, vol. 21, no. 11, pp. 469–471, 1985.

[15] J. Harari, D. Decoster, J. P. Vilcot, B. Kramer, C. Oguey, P. Salzac, and G. Ripoche, "Numerical simulation of avalanche photodiodes with guard ring," *IEE Proc-J*, vol. 138, no. 3, pp. 211–217, 1991.

Improvements of the Two-Dimensional FDTD Method for the Simulation of Normal- and Superconducting Planar Waveguides Using Time Series Analysis

Stefan Hofschen and Ingo Wolff

Abstract— **Time-domain simulation results of two-dimensional (2-D) planar waveguide finite-difference time-domain (FDTD) analysis are normally analyzed using Fourier transform. The introduced method of time series analysis to extract propagation and attenuation constants reduces the desired computation time drastically. Additionally, a nonequidistant discretization together with an adequate excitation technique is used to reduce the number of spatial grid points. Therefore, it is possible to simulate normal- and superconducting planar waveguide structures with very thin conductors and small dimensions, as they are used in MMIC technology. The simulation results are compared with measurements and show good agreement.**

Manuscript received September 9, 1994; revised April 19, 1996.

The authors are with the Department of Electrical Engineering, Gerhard Mercator University of Duisburg, Duisburg, Germany.

Publisher Item Identifier S 0018-9480(96)05657-8.

I. INTRODUCTION

Recently, a two-dimensional finite-difference time-domain (2-D-FDTD) algorithm has been introduced as an efficient full-wave analysis method for arbitrarily shaped waveguide structures [1]. Normally, the simulation results are extracted from the time series using Fourier transform. For very small structures and thin conductors, as they are used in the MMIC technology, a very fine spatial discretization is required. Due to the stability condition of the FDTD technique, the fine spatial discretization causes a very fine time discretization, too.

In this work we introduce a time series analysis technique using a Powell optimization technique to extract dispersion and loss characteristics of planar waveguiding structures from only a part of a single period of the time signal. Especially if the fields inside the conductors have to be calculated to analyze the waveguide losses, the method reduces the required computation time up to a factor of 25. Therefore, it is possible to simulate planar and coplanar waveguides with a metallization thickness of only 2 μm or a superconducting film thickness of 300 nm, which cannot be simulated with the conventional FDTD or 2-D-FDTD techniques due to the enormous CPU time needed.

II. THEORY

For the 2-D-FDTD algorithm, the spatial derivatives for the transverse fields in one direction, e.g., the x-direction, which should be the propagation direction of the guided wave, are replaced using the analytical formulas [1]

$$\underline{\vec{E}}_t(x \pm \Delta x) = \underline{\vec{E}}_t(x) \cdot e^{\mp \jmath \beta \Delta x}$$

$$\underline{\vec{H}}_t(x \pm \Delta x) = \underline{\vec{H}}_t(x) \cdot e^{\mp \jmath \beta \Delta x}. \tag{1}$$

Thus, 2-D-FDTD mesh formulation can be derived. During the simulation, a propagation constant β and a proper excitation are chosen. After a certain number of iterations, the corresponding modal frequencies can be extracted using Fourier transform of the time series obtained. In the conventional approach, repeating the Fourier transform after some iterations makes it possible to calculate the losses of the waveguiding structure. For the 2-D-FDTD method, a new stability condition can be derived under the assumption that $\Delta x \rightarrow 0$ [2]

$$c_0 \Delta t = \left[\frac{1}{(\Delta y)^2} + \frac{1}{(\Delta z)^2} + \left(\frac{\beta}{2} \right)^2 \right]^{-\frac{1}{2}}. \tag{2}$$

It can be seen that the time step Δt depends on the maximum wave phase velocity c_0 in the air-filled region above the dielectric substrate, and mainly on the spatial discretizations Δy and Δz. The discretizations Δy and Δz inside the conducting material should be smaller than the skin depth in the case of a normal conductor, or smaller than the London penetration depth in the case of a superconductor for the given material and frequency. Due to the extreme short corresponding time step Δt, a tremendous number of iterations is necessary to obtain the time series of voltage and current on the waveguide for at least one period. The simulations demonstrated in the following would, e.g., require at least 10^5 iteration steps for one period at 8 GHz, using a discretization of 0.5 μm. Keeping in mind that several periods are necessary for an exact Fourier transform, the simulation of such a structure becomes nearly impossible using the conventional technique. The

major ideas to reduce the required computation time are the usage of a nonequidistant discretization of the spatial domain and a specialized method to extract the desired propagation constants of the planar waveguides after only a small number of time steps.

III. Discretization

Normally, in the FDTD method, a very simple excitation field, e.g., an unidirectional, homogeneous electric field inside the slot between the conductors of a CPW, is used as the starting condition for the simulation. If such a simple excitation is used, wave components are enforced that are not part of the normal guided wave solution of the investigated waveguide. For the 2-D-FDTD, these wave components are initiated as a kind of cylindrical wave or pulse, propagating from the excitation point to the outer boundaries of the computational domain. A problem occurs if a nonequidistant, graded mesh which is strongly recommended for the simulation of MMIC waveguides is used perpendicular to the propagation direction. The loss of second-order accuracy causes the cylindrical waves and pulses to be multiply reflected at the mesh discontinuities. Additionally, the waves and pulses initiated in the fine mesh regions cannot propagate into the regions with the coarse mesh and are therefore strongly reflected.

These disturbances can be suppressed if a field distribution, e.g., calculated from a quasi-static finite-difference-method (FDM) is used as the excitation condition for the 2-D-FDTD. In the FDM, a nonequidistant discretization can also be easily taken into account and, therefore, nearly no disturbing field components will be initiated in the 2-D-FDTD. The small disturbances due to the transition from the quasistatic FDM to the dynamic FDTD analysis will fade away after a short simulation time and will not hinder the calculation of currents and voltages. Thus, a graded mesh can be used without introducing additional computational steps as proposed in [3], only a short time for the precalculation using the FDM is needed.

IV. Time Series Analysis

If a CPW is simulated, a magnetic wall is introduced in the symmetry plane of the structure whereby the odd mode is suppressed. Thus, a nearly monomodal response to the excitation can be achieved. In this case, it is known *a priori* that the time series resulting from the simulation will be a damped sinusoidal wave if losses are incorporated, too. Hence, the theoretical time signal can be fitted to the simulation results, after only a time of 1/15 up to 1/2 of one cycle duration which leads to a drastically reduced CPU time. The current on the center strip of a CPW has been determined and stored for each time step by evaluating the line integral along a closed contour c around the center strip

$$i(n\Delta t) = \oint_c \vec{H}(y,\, z,\, n\Delta t)\, d\vec{s}. \tag{3}$$

The theoretical time signal

$$i(n\Delta t) = x_1 e^{-x_4 n} \cos\left(\frac{2\pi}{x_2}(n + x_3)\right) \tag{4}$$

has been fitted to the simulated data, using a Powell optimization technique [4] with the optimization variables x_1 to x_4. The relative error for each data point is less than 10^{-4} which shows that the response really is a single-frequency signal. The same procedure is applied to the voltage between the inner and outer conductor. From the variables x_1, x_2, x_4 and the frequency $f = 1/(x_2\Delta t)$, the magnitude of the characteristic impedance $|Z_c|$, the effective dielectric constant ϵ_{reff} corresponding to the chosen β and the attenuation constant α can be calculated by

$$\sqrt{\epsilon_{reff}} = \frac{c_0 \Delta t}{2\pi}\beta x_2 \tag{5}$$

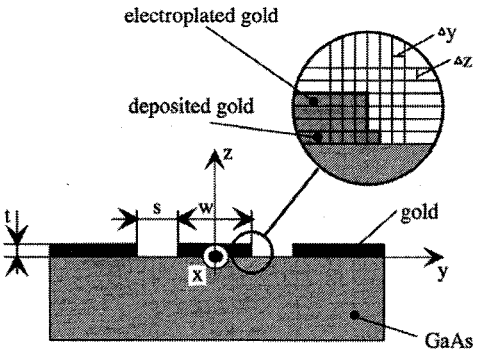

Fig. 1. The simulated CPW structure.

$$|Z_c| = \frac{\hat{u}}{\hat{1}} \tag{6}$$

$$\alpha = \frac{x_4\sqrt{\epsilon_{reff}}}{c_0 \Delta t} \tag{7}$$

where $\hat{u}$ and $\hat{1}$ are the amplitudes of the voltage and current on the waveguide which can be evaluated from the corresponding value x_1 for u and i, respectively. All simulations have been carried out on a RISC R4400 workstation. The required CPU time has been determined to be approximately 2.2 s per 1000 time steps and 1000 mesh points. As an example for the structure corresponding to Figs. 1 and 2, the number of time steps and the CPU time required per frequency point for different frequencies including the optimization time are given in Table I. The total number of time steps and the total CPU time for all structures are presented in Table II, together with an average value for the CPU time per frequency point. The desired memory space has been between 2 and 3 Mbytes for all examples.

V. Simulation and Measurements of CPW's on GaAs

In Fig. 2, the simulation and measuring results for a CPW on GaAs are shown. For this structure, the different dimensions of the first deposited gold layer and the electroplated second gold layer, as shown in Fig. 1, have been taken into account. The thickness of the first layer is 0.5 μm and the conductivity is only 70% of the second layer's conductivity $\kappa = 35.4 \cdot 10^6$ 1/Ω m. All these data have been taken directly from the technological process description. The spatial resolution of the applied 2-D-FDTD analysis has been chosen to be 1/4 of the metallization thickness t. The agreement between simulation and measurement especially concerning ϵ_{reff} (Fig. 2) is excellent, and the occurring deviations are comparable to the errors in the fabrication and measuring process.

From Fig. 2(b), it can be seen that the attenuation coefficient calculated by FDM is only valid below 20 GHz. The deviation of the results, obtained by the 2-D-FDTD technique, from the measurement near and above 38 GHz, can be explained by the fact that at these frequencies the skin depth is nearly equal to the minimal discretization length Δz.

To analyze the influence of the first layer, the same structure has been simulated under the assumption that inner and outer conductors are of an ideal rectangular cross section. While the deviation for the attenuation coefficient α is only significant for frequencies above 20 GHz, the effective dielectric constant differs at least 2.5% from the original values in the total considered frequency range.

VI. Simulation and Measurements of Superconducting CPW's

Due to the strong influence of the kinetic inductance in superconducting planar waveguides, it is very important to take the field

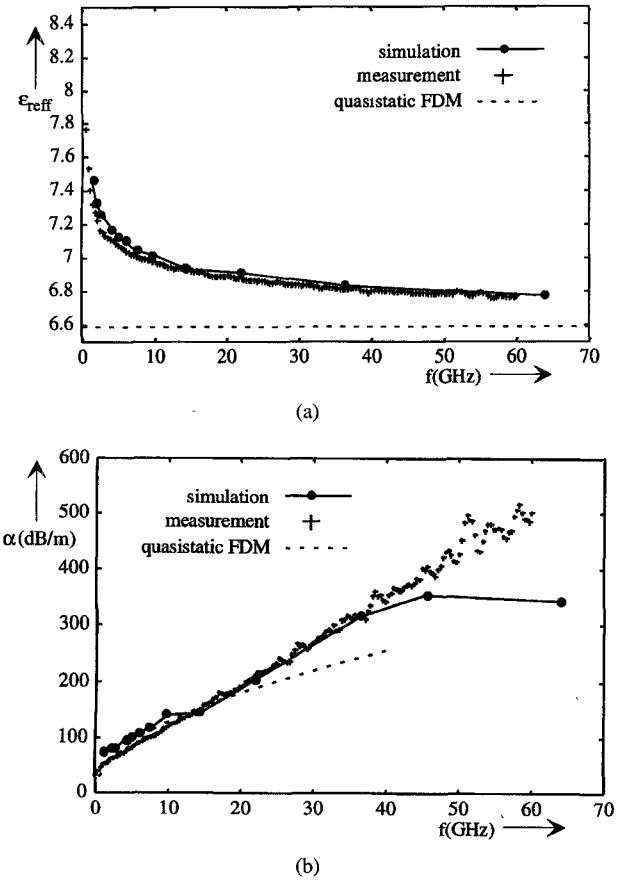

Fig. 2. Effective dielectric constant ϵ_{reff} (a) and attenuation coefficient α (b) of the CPW on GaAs ($\epsilon_r = 12.9$) shown in Fig. 1 as a function of frequency. Parameters: $w = 30$ μm, $s = 25$ μm, $t = 2$ μm, $\Delta z = 0.5$ μm, $\Delta y = 1.0$ μm.

TABLE I
NUMBER OF TIME STEPS AND CPU TIME PER FREQUENCY POINT FOR THE STRUCTURE IN FIG. 1

frequency range	timesteps	CPU-time, min
< 4GHz	80,000	18
~15GHz	25,000	7
~65GHz	6,000	3

TABLE II
TOTAL NUMBER OF TIME STEPS AND CPU TIME FOR ALL EXAMPLES

example	timesteps	mesh size	frequency points	av. time/fr. point, min
Figs. 1, 2	600,000	70x80	12	11
Fig. 3	1,172,000	70x100	13	30

penetration inside the superconducting film into account to calculate the effective dielectric constant and the losses of such a CPW accurately. In this case, the requirements for a simulation method are even higher than for normal conductors, because of the very small film thickness of 300 nm. Additionally, the London penetration depth is only about 150 nm at low temperatures. Therefore, a discretization of only 75 nm inside the conductor was chosen for this example. The effective dielectric constant ϵ_{reff} of a superconducting CPW fabricated from YBaCuO on a $LaAlO_3$ substrate has been measured,

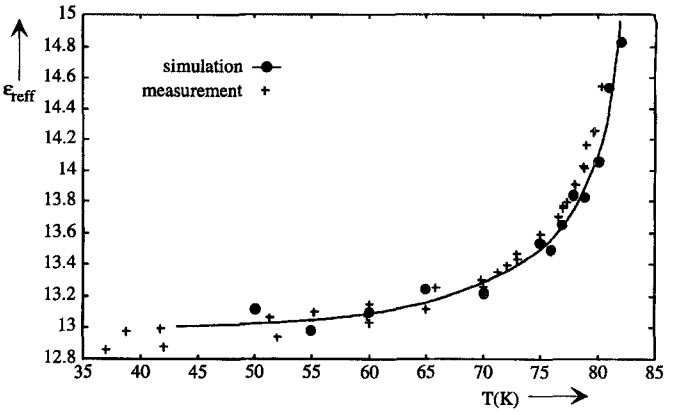

Fig. 3. Simulated and measured effective dielectric constant ϵ_{reff} of a superconducting CPW on $LaAlO_3$ ($\epsilon_r = 24.5$) as a function of temperature. Parameters: $w = 10$ μm, $s = 20$ μm, $\Delta y = 660$ nm, $\Delta z = 75$ nm.

using a CPW resonator technique at 15 GHz [5]. The center strip was 10 μm and the gap 20 μm wide to obtain $Z_c = 50$ Ω. The critical temperature after the fabrication was 86K and the London penetration depth λ_L ($T = 0$K) was 150 nm. For the simulation of the superconductor, the London theory has been introduced into the 2-D-FDTD following the approach of [6]. Using a complex conductivity $\sigma = \sigma_1 - j\sigma_2$, a new time domain formulation of Maxwell's equation can be derived:

$$\nabla \times \vec{H} = \sigma \vec{E} + \frac{\partial}{\partial T}\epsilon \vec{E} + \frac{1}{\mu_0 \lambda_L^2}\int_0^t \vec{E}\, dt. \tag{8}$$

If this equation is discretized as proposed in [6], some stability problems will occur for good superconductors with small λ_L. For the one-dimensional plane wave propagation, the additional stability condition has been found to be $\Delta x < 0.5\lambda_L$ [7].

In [8] it has been proposed to solve this problem by using $\sigma_1 \vec{E}^{(n+1)}$ for $\sigma_1 \vec{E}$ when discretizing (8). In this case, the stability depends on the absolute value of the normal conductivity σ_1 of the superconductor, and therefore no better stability can be achieved for very good superconductors or near $T = 0$K, where $\sigma_1 \to 0$.

For the simulation presented in this paper, another method is used. The time integral at $t = n\Delta t$ mainly representing the superconducting properties has been transformed using

$$\int_0^t \vec{E}\, dt \to \Delta t \sum_{i=0}^{n+1} \vec{E}^{(i)}. \tag{9}$$

Thus, stability for all combinations of σ_1, λ_L, and Δx has been achieved.

Fig. 3 shows the simulation and measuring results. They are in good agreement, and the field penetration seems to be well modeled over the whole temperature range. ϵ_{reff} changes about 15% in this temperature range, due to the strong increase of the London penetration depth and the resultant kinetic inductance. Therefore, a prediction of this behavior will be very important to guarantee an accurate circuit design.

VII. CONCLUSION

A new method for a time series analysis of two-dimensional FDTD simulation results has been demonstrated. In combination with an adequate excitation technique and the usage of a graded mesh, this method allows us to simulate planar and coplanar structures with very thin conductor thicknesses and small dimensions, as they are used in the MMIC technology. Additionally, superconducting CPW's have been analyzed with discretizations down to 75 nm. In all examples,

a good agreement between the measuring results and the simulations has been observed and the advantage of a very find discretization has been shown. In the future, this method can be a powerful tool to calculate losses and propagation constants for planar MMIC waveguides, especially at high frequencies with a drastically reduced amount of computation time.

REFERENCES

[1] V. J. Brankovic, D. V. Krupezevic, and F. Arndt, "An efficient two-dimensional graded mesh finite-difference time-domain algorithm for shielded or open waveguide structures," *IEEE Trans. Microwave Theory Tech.*, vol. 40, pp. 2272–2277, Dec. 1992.

[2] A. C. Cangellaris, "Numerical stability and numerical dispersion of a compact 2-D/FDTD method used for the dispersion analysis of waveguides," *IEEE Microwave Guided Wave Lett.*, vol. 3, pp. 3–5, Jan. 1993.

[3] S. Xiao and R. Vahldieck, "An improved 2-D-FDTD algorithm for hybrid mode analysis of quasiplanar transmission lines," in *1993 IEEE MTT-S Dig.*, pp. 421–424.

[4] W. H. Press, S. A. Teukolsky, W. T. Vetterling, and B. P. Flannery, *Numerical Recipes in C.* Cambridge: University Press, 1992.

[5] S. Hofschen, I. Wolff, and U. Salz, "Determination of propagation and attenuation constants of superconducting coplanar waveguides for the design of MIC using stripline resonator measurements," in *Proc. 1993 European Conf. Appl. Superconductivity*, Goettingen, Germany, Oct. 1993.

[6] M. Rittweger and I. Wolff, "Finite difference time-domain formulation of transient propagation in superconductors," in *IEEE APS Int. Symp. Dig.*, July 1992, pp. 1960–1963.

[7] S. Hofschen, I. Wolff, E. Waffenschmidt, J. Berntgen, and K. Heime, "Using the 2-D-FDTD method for the accurate analysis of superconducting coplanar waveguides and the design of planar rectangular inductors," in *Proc. 25th European Microwave Conf.*, Sept. 1995, pp. 755–760.

[8] S. Xiao and R. Vahldieck, "An extended 2-D-FDTD method for hybrid mode analysis of lossy and superconducting structures," in *IEEE APS Int. Symp. Dig.*, July 1994, pp. 1774–1777.

Three-Port Hybrid Power Dividers Terminated in Complex Frequency-Dependent Impedances

Stanislaw Rosloniec

***Abstract*—A new CAD algorithm for design of two- and four-section three-port hybrid power dividers terminated with complex frequency-dependent impedances is described. The dividers under consideration are composed of lumped element resistors and noncommensurate transmission line sections whose characteristic impedances take extreme, practically realizable, values. These values are assumed freely at the beginning of a design process. The validity of the presented design algorithm has been confirmed by numerical modeling and experimentation.**

I. INTRODUCTION

The hybrid power dividers (combiners) of Wilkinson type are widely used in various UHF and microwave devices intended to work at small and medium power levels. As a rule, those dividers are terminated with the same frequency-independent resistances, usually equal to 50 Ω. Typical examples of such divider designs are described in the commonly available literature (see [1]–[4] for instance). In contrast to that, [5] and [6] present algorithms for designing similar dividers whose ports are loaded by different but also constant resistances. In some applications, however, it may be advantageous to use the dividers terminated with different and frequency-dependent complex impedances. By way of example, the combiners of that type are especially desirable for broad-band equiphase array antennas. Unfortunately, the design and hardware implementation of broad-band microwave dividers terminated in complex impedances have not as yet been sufficiently investigated in the literature. Therefore, this paper is a contribution to solve that practically important problem. A new CAD algorithm for design of novel Wilkinson dividers is described. The proposed dividers are composed of noncommensurate transmission line sections and lumped element resistors. It should be pointed out that characteristic impedances of these line sections are limited on both sides, i.e., by impedances $Z_{0\min}$ and $Z_{0\max}$ assumed freely at the beginning of a design process. Due to that, they may be easily realized, for example, of microstrip line segments. The validity of the proposed design method has been confirmed by numerical modeling and experimentation.

Manuscript received January 7, 1995; revised April 19, 1996.

The author is with the Institute of Radioelectronics, Warsaw University of Technology, Nowowiejska 15/19, 00-665 Warsaw, Poland.

Publisher Item Identifier S 0018-9480(96)05656-6.

II. DESIGN PROCEDURE

The strip line topologies of two- and four-section power dividers considered here are shown in Figs. 1(a) and 2(a), respectively. These divider circuits have mirror-reflection symmetry (with respect to planes $x-x'$), so they can be analyzed by means of the even- and odd-mode excitations method [7], [3]. Consequently, we obtain two pairs of bisection two-port circuits whose electrical schemes are shown also in Figs. 1 and 2. According to [1]–[3], [5], the scattering parameters $[S(f)]$ of power dividers under analysis may be expressed in terms of the scattering parameters $[S^{++}(f)]$ and $[S^{+-}(f)]$ evaluated for the corresponding even- and odd-mode two-port circuits. The suitable relationships are

$$\begin{aligned} S_{11}(f) &= S_{11}^{++}(f) \\ S_{12}(f) &= S_{21}(f) = S_{13}(f) = S_{31}(f) = S_{12}^{++}(f)/\sqrt{2} \\ S_{22}(f) &= S_{33}(f) = [S_{22}^{++}(f) + S_{22}^{+-}(f)]/2 \\ S_{23}(f) &= S_{32}(f) = [S_{22}^{++}(f) - S_{22}^{+-}(f)]/2. \end{aligned} \tag{1}$$

It is evident from Figs. 1(b) and 2(b) that even-mode two-ports serve as broad-band stepped transmission line matching circuits included between the complex admittances $Y_g(f)/2$ and $Y_l(f)$. In this paper, the method published in [8] has been chosen for the design of these distributed element matching circuits. As it results from the relationships in (1), the divider characteristic $S_{11}(f)$ is unequivocally determined by the scattering parameter $S_{11}^{++}(f)$, i.e., indirectly by admittances $Y_g(f)/2, Y_l(f)$ and electrical parameters of the matching circuit connecting them. In other words, the characteristic $S_{11}(f)$ is independent of the isolating resistors. This feature allows us to shape the isolation characteristic $I(f)[\text{dB}] = 20\log[1/|S_{23}(f)|]$ between divider ports 2 and 3 without distortion of the input return loss characteristic $S_{11}(f)[\text{dB}] = 20\log[|S_{11}(f)|]$ achieved earlier. Therefore, let us assume that characteristic impedances and electrical lengths of the line sections creating the divider are known [8]. Then, the next nontrivial problem of the design is to calculate the isolating resistors such that characteristics $I(f)[\text{dB}]$ and $S_{22}(f)[\text{dB}] = S_{33}(f)[\text{dB}] = 20\log[|S_{22}(f)|]$ will be optimum [3]–[5], [9]. It has been found numerically that this optimization problem may be successfully solved by using the minimization method presented